ACS APPLIED MATERIALS & INTERFACES

Research Article

www.acsami.org

Synergistic Dual-Modality *in Vivo* Upconversion Luminescence/X-ray Imaging and Tracking of Amine-Functionalized $NaYbF_4$:Er Nanoprobes

Zhigao Yi,[†,‡] Songjun Zeng,[*,†] Wei Lu,[§] Haibo Wang,[†,‡] Ling Rao,[†,‡] Hongrong Liu,[†] and Jianhua Hao[*,§]

[†]College of Physics and Information Science and Key Laboratory of Low-Dimensional Quantum Structures and Quantum Control of the Ministry of Education, Hunan Normal University, Changsha, Hunan 410081, People's Republic of China

[‡]Faculty of Materials, Optoelectronics and Physics, Key Laboratory of Low-Dimensional Materials and Application Technology (Ministry of Education), Xiangtan University, Xiangtan 411105, People's Republic of China

[§]Department of Applied Physics and Materials Research Center, The Hong Kong Polytechnic University, Hong Kong

ABSTRACT: In this work, the amine-functionalized $NaYbF_4$:Er nanoparticles were developed as dual-modal nanoprobes for synergistic upconversion (UC) luminescence and X-ray imaging in a single system by a simple one-step method of simultaneous synthesis and surface modification. The water-soluble $NaYbF_4$:Er nanoparticles present excellent green and dominant red UC emissions. The *in vitro* cell imaging shows that the high-contrast green and intense red UC emissions can be observed from HeLa cells treated with these nanoparticles, indicating the successful labeling of HeLa cells. Moreover, the localized spectra measured from HeLa cells and background presented significant green and dominant red UC emissions with the absence of any autofluorescence, further verifying that these nanoparticles can be successfully used as ideal probes for optical UC bioimaging with high contrast and non-autofluorescence. In addition, the amine-functionalized $NaYbF_4$:Er nanoparticles maintained low cell toxicity in HeLa cells evaluated by the 3-(4,5-dimethylthiazol-2-yl)-2,5-diphenyltetrazolium bromide (MTT) assay. More importantly, these amine-functionalized $NaYbF_4$:Er nanoparticles can also be used as X-ray imaging, owing to the large X-ray absorption efficiency of the Yb ion. The synergistic *in vivo* UC and X-ray imaging present significant UC luminescence and X-ray signals in the same region of a nude mouse, and the two signals are matched very well, which provides direct evidence for simultaneous UC luminescence and X-ray imaging in a single compound of lanthanide-doped material. Moreover, *ex vivo* UC imaging shows that these nanoparticles are first accumulated in the lung and gradually translocated from the lung into the liver. These results demonstrate that the amine-functionalized $NaYbF_4$:Er nanoparticles presented here are very attractive nanoprobes for dual-modal UC luminescence and X-ray imaging with low cytotoxicity, autofluorescence free, and synergistic combination of the advantages of the two imaging modalities.

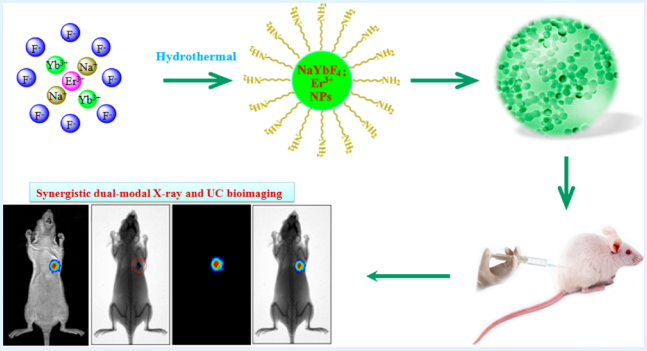

KEYWORDS: *upconversion nanoparticle, upconversion luminescence bioimaging, X-ray imaging, synergistic dual-modality bioimaging*

1. INTRODUCTION

Optical bioimaging plays an important role in biomedical study, visualization, and understanding of the function of specific molecules and tissues.[1−5] Upconversion nanoparticles (UCNPs) have emerged as a new generation of nanoprobes for optical bioimaging, owing to the ability of converting longer wavelength excitation to shorter wavelength emissions.[6−14] In comparison to the previously developed traditional fluorescent probes, such as organic dyes, fluorescent proteins, and quantum dots (QDs),[15−17] UCNPs possess many advantages, including large anti-Stokes shifts, long lifetimes, high photostability, reduced auto-fluorescence, no blinking, and deep tissue penetration.[18−42] It is noted that host material of UCNPs has played a vital role in achieving efficient UC luminescence. Among the previously developed UC host materials, fluorides ($NaLnF_4$, where Ln = rare earth elements) are considered as ideal hosts for UC emissions, owing to their low phonon energy.[43] However, much efforts have focused on developing the lanthanide-doped $NaYF_4$ UCNPs for the UC luminescence bioimaging of cells and tissues *in vitro* and *in vivo*.[44−47] Unfortunately, sodium ytterbium fluoride ($NaYbF_4$) as an important fluoride has obtained limited research. A recent report indicated that the intensity of the near-infrared (NIR) UC emission of $NaYbF_4$:Tm^{3+} is 43 times higher than that of $NaYF_4$:Yb^{3+}/Tm^{3+} and the synthesized ultra-small $NaYbF_4$:2% Tm^{3+} nanocrystals with the size of 10 nm can significantly emit

Received: October 15, 2013
Accepted: March 5, 2014
Published: March 5, 2014

enhanced NIR emission compared to $NaYF_4$:20% Yb^{3+}/2% Tm^{3+} nanocrystals with the size of 25−30 nm.[48] Our previous reports[49,50] also revealed that $NaYbF_4$:Er^{3+} is capable of emitting dominant red UC emission, owing to the large Yb^{3+} content, which is in contrast to the dominant green UC emission usually observed in $NaYF_4$:Yb^{3+}/Er^{3+}. Such an UC spectroscopy would be more beneficial for *in vivo* deeper tissue optical bioimaging.[51] Despite the promising UC property and preliminary studies on lanthanide-doped $NaYbF_4$ UCNPs reported, optical bioimaging using the novel system of UCNPs has not yet been demonstrated.

On the other hand, apart from the aforementioned excellent UC property, the Yb-based host can also act as a potential contrast agent for X-ray imaging, owing to the large X-ray absorption coefficients of the Yb element (at 80 keV, Yb = 6.91 cm^2 g^{-1})[52] and K-edge values ($Yb_{K\text{-}edge}$ = 61 keV).[53,54] Therefore, in comparison to the well-developed $NaYF_4$ host, the $NaYbF_4$ host possesses some intrinsic advantages, including (1) the larger K-edge energy (61 keV), located in higher energy regions for X-ray imaging and resulting in higher intrinsic contrast and a lower radiation exposure to patients, and (2) Yb^{3+} being a well-known sensitizer in UC luminescence and significantly enhancing the red UC emission in the Er^{3+}-doped $NaYbF_4$ host, which is beneficial for optical bioimaging. Therefore, the excellent UC property in combination with the large X-ray absorption property makes the lanthanide-doped $NaYbF_4$ host attractive for dual-modal UC luminescence and X-ray imaging in biomedical application. However, there has been little study on the development of the $NaYbF_4$ dual-modal nanoprobe for UC luminescence and X-ray imaging, especially for synergistic UC luminescence and X-ray imaging in a single system.

In this paper, the high-quality amine-functionalized $NaYbF_4$:Er UCNPs were synthesized by a simple one-step hydrothermal method using some low-toxicity solvent. These UCNPs were used for *in vitro* optical bioimaging of HeLa cells. The cytotoxicity in HeLa cells was also evaluated. More importantly, the synergistic UC luminescence and X-ray imaging in the same region of a nude mouse was demonstrated using these UCNPs for the first time.

2. EXPERIMENTAL SECTION

2.1. Chemicals and Materials. $Ln(NO_3)_3{\cdot}6H_2O$ (Ln = Yb and Er, at 99.99%) and polyethylenimine (PEI, 25 kDa) were purchased from Sigma-Aldrich. Ethylene glycol (EG) and sodium fluoride were obtained from Sinopharm Chemical Reagent Co., China. All of these chemicals were used without further purification.

2.2. Synthesis of the Amine-Functionalized $NaYbF_4$:Er Nanoparticles. Through a modified one-step hydrothermal method,[55] the water-soluble amine-functionalized $NaYbF_4$:Er UCNPs were synthesized. Typically, 1 mmol of $Yb(NO_3)_3$ (0.5 M) and $Er(NO_3)_3$ (0.1 M) with the designed molar ratio of 98:2 was added to 30 mL of EG containing 1.0 g of PEI to obtain homogenous transparent solution by vigorously stirring. Then, 4.5 mmol of NaF (1 M) was added to the above mixture after stirring for another 30 min. Finally, the obtained solution was transferred into a 50 mL stainless Teflon-lined autoclave and maintained at 190 °C for 24 h. The system was cooled to room temperature naturally after the reaction finished completely. The final products were separated by centrifugation, washed several times with ethanol and de-ionized water, and then dried at 60 °C for 24 h.

2.3. Characterization. The crystal phase of the amine-functionalized $NaYbF_4$:Er UCNPs was recorded by powder X-ray diffraction (XRD) using a Bruker D8 advance X-ray diffractometer (40 kV and 200 mA) with Cu Ka radiation (λ = 1.5406 Å). Transmission electron microscopy (TEM) (JEOL-2100F) equipped with the energy-dispersive X-ray spectrum (EDS) was used to characterize the size and shape of the as-prepared UCNPs. The surface ligands of the as-prepared UCNPs were detected by Fourier transform infrared spectrum (FTIR) using a Magna 760 spectrometer E.S.P. (Nicolet). An UC luminescence spectrum was obtained by a FLS920P Edinburgh Analytical Instrument apparatus equipped with a 980 nm laser diode at room temperature. The digital photograph of the as-prepared UCNPs water solution (1 wt %) was taken by a Canon digital camera under the excitation of a 980 nm laser with a power density of 5 W/cm^2.

2.4. Cell Culture. HeLa cells were cultured in Dulbecco's modified Eagle's medium (DMEM) supplemented with 10% fetal bovine serum (FBS), 1% penicillin and streptomycin at 37 °C, and 5% CO_2.

2.5. *In Vitro* Optical UC Bioimaging. The *in vitro* UC luminescence bioimaging of the amine-functionalized $NaYbF_4$:Er UCNPs in HeLa cells was carried out by a confocal laser scanning microscope (Leica TCS SP5) under the excitation of a 980 nm wavelength laser. HeLa cells were incubated with 200 μg mL^{-1} concentration of UCNPs at 37 °C and 5% CO_2 for 24 h. Two typical emission channels at green (500−600 nm) and red (600−700 nm) spectral regions were detected.

2.6. Cytotoxicity Assay. The cell toxicity of these UCNPs in HeLa cells was evaluated by a 3-(4,5-dimethylthiazol-2-yl)-2,5-diphenyltetrazolium bromide (MTT) proliferation method. HeLa cells were seeded into a 96-well microplate (6000 cells/well) and pre-incubated at 37 °C under 5% CO_2 for 4 h. Then, the cell culture medium in each well was replaced by DMEM solutions containing various concentrations of the amine-functionalized $NaYbF_4$:Er UCNPs (200, 500, 1000, and 2000 μg/mL). Then, HeLa cells treated with UCNPs were incubated at 37 °C under 5% CO_2 for another 24 h. The absorbance band centered at 570 nm was measured by Multiskan EX (Thermo Electron Corporation).

2.7. *In Vivo* UC Bioimaging. For the purpose of testing the feasibility of the *in vivo* UC bioimaging based on these UCNPs, a nude mouse that was anesthetized by intraperitoneal injection of 10 wt % chloral hydrate solution was subcutaneously injected 200 μL of the amine-functionalized $NaYbF_4$ UCNPs aqueous solution (2 mg/mL). After injection, *in vivo* UC bioimaging was performed by an *in vivo* imaging system (Bruker In-Vivo FX PRO) equipped with an external fiber-coupled 980 nm laser. The UC bioimaging was captured using a band pass filter (650/50 nm) with an exposure time of 5 s.

2.8. Simultaneous *in Vivo* X-ray and UC Bioimaging. To demonstrate the dual-modal imaging functionality of these UCNPs, the simultaneous *in vivo* X-ray and UC imaging was carried out in the same nude mouse subcutaneously injected 200 μL of the amine-functionalized $NaYbF_4$ UCNPs aqueous solution (2 mg/mL). The simultaneous X-ray and UC imaging was detected by the multi-modal *in vivo* imaging system (Bruker In-Vivo FX PRO) equipped with an X-ray imaging functionality with an operating voltage of 0−35 kVp. The UC signal was detected at a red emission region by a band pass filter (650/50 nm), and the X-ray imaging was recorded under the operating voltage of 35 kVp (0.4 filter, with an exposure time of 1 min).

2.9. *Ex Vivo* UC Optical Imaging. To reveal the distribution and translocation of these UCNPs in major organs, two nude mice were first intravenously injected with these UCNPs (2 mg/mL, 200 μL). After 0.5 and 24 h of injection, the two mice were dissected and the UC signals of some major organs, such as the heart, lung, liver, spleen, and kidney, were detected by the *in vivo* imaging system (Bruker In-Vivo FX PRO) using similar experimental conditions with aforementioned *in vivo* UC imaging.

3. RESULTS AND DISCUSSION

3.1. Structure Characterization. In this work, water-soluble $NaYbF_4$:Er UCNPs modified by an amine ligand were synthesized using PEI as the capping agent. Figure 1 shows the typical XRD pattern of the as-prepared UCNPs. As shown in Figure 1, all of the characteristic diffraction peaks are matched well with the standard cubic phase $NaYbF_4$ [Joint Committee on Powder Diffraction Standards (JCPDS) number 77-2043] and no other impurity diffraction peaks are observed, indicating

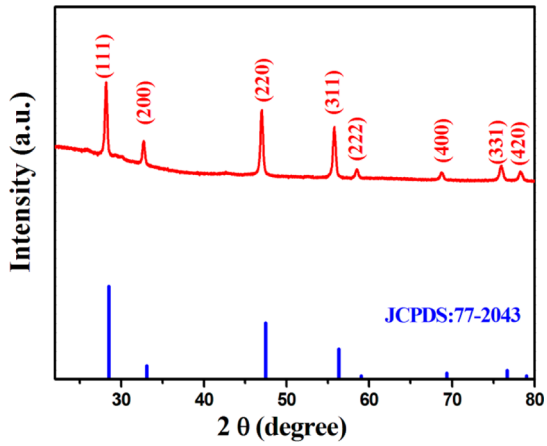

Figure 1. XRD patterns of the amine-functionalized $NaYbF_4$:Er UCNPs. The red line is experimental diffraction data, and the blue line indicates the standard cubic phase $NaYbF_4$ (JCPDS number 77-2043).

the formation of pure cubic phase $NaYbF_4$. To further reveal the shape and size of the as-prepared UCNPs, TEM characterizations were performed. As demonstrated in Figure 2a, the as-prepared UCNPs present sphere-like shape. The inset of Figure 2a shows the typical size-distribution of the as-prepared UCNPs, demonstrating the average size of about 28 ± 2.4 nm. Figure 2b shows the corresponding selected area electron diffraction (SAED) pattern, further verifying the face-centered cubic (FCC) phase structure of the as-prepared UCNPs, which is consistent with the aforementioned XRD analysis. The high-resolution TEM of the individual nanoparticle (Figure 2c) shows that the as-prepared UCNPs possess high crystallinity with a measured *d* spacing of 1.92 Å, corresponding to the (220) lattice plane of the cubic phase $NaYbF_4$. The element composition of the as-prepared UCNPs was detected by EDS (Figure 2d). As demonstrated, the as-prepared UCNPs are mainly composed of Na, Yb, and F, which further validates the formation of $NaYbF_4$. It should be noted that the Cu and C signals are attributed to the Cu grid of TEM and no signal of the doped 2% Er is mainly ascribed to the limited detection precision.

3.2. FTIR Analysis. Amine functionalization selected here can not only improve the water-solubility of the nanoparticles but also enhance the cellular uptake by endocytosis.[56] To test the surface ligand of the as-prepared UCNPs, FTIR analysis was performed. Figure 3 shows the typical FTIR spectrum of the amine-functionalized $NaYbF_4$:Er UCNPs. As demonstrated, two typical weak absorption peaks centered at 2924 and 2841 cm^{-1} are observed, corresponding to the asymmetric and symmetric stretching vibrations of the C−H bond, respectively. The strong absorption bands located at 1636 and 3449 cm^{-1} were attributed to the N−H bending mode of amino group ($-NH_2$)[57] and the stretching vibration of amine groups, respectively. It indicates the successful grafting of the amine ligand on the surface of UCNPs.

3.3. UC Photoluminescence Properties. The UC spectrum of the amine-functionalized $NaYbF_4$:Er UCNPs was detected under the excitation of a 980 nm laser diode at room temperature. As demonstrated in Figure 4a, the amine-functionalized $NaYbF_4$:Er UCNPs present weak green UC emissions centered at 521/540 nm and dominant red UC emission centered at 651 nm. As shown in the energy level diagram (Figure 4b), under 980 nm excitation, the electrons in

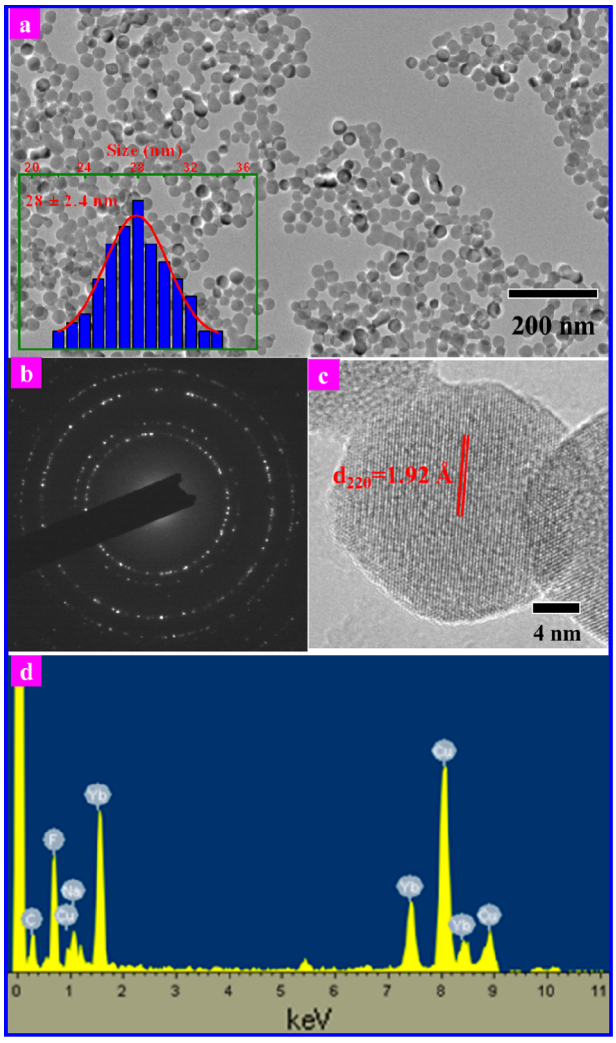

Figure 2. TEM and EDS results of the amine-functionalized $NaYbF_4$:Er UCNPs: (a) typical TEM image, (b) corresponding SAED pattern, indicating the FCC phase structure, (c) high-resolution (HR)-TEM image of an individual particle, and (d) EDS. The inset in panel a presents the size distribution of the nanoparticles.

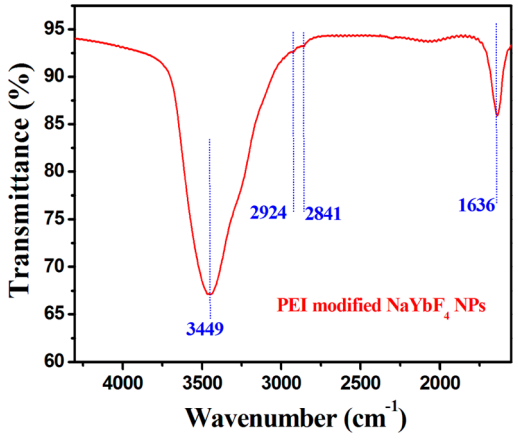

Figure 3. Typical FTIR spectrum of the amine-functionalized $NaYbF_4$:Er UCNPs.

the Yb^{3+}:$^2F_{7/2}$ level are excited to the excited state of the $^2F_{5/2}$ level. When the electrons in the Yb^{3+}:$^2F_{7/2}$ level return to the ground state, the efficient energy transfers occurred from Yb^{3+}

dx.doi.org/10.1021/am500383m | ACS Appl. Mater. Interfaces 2014, 6, 3839−3846

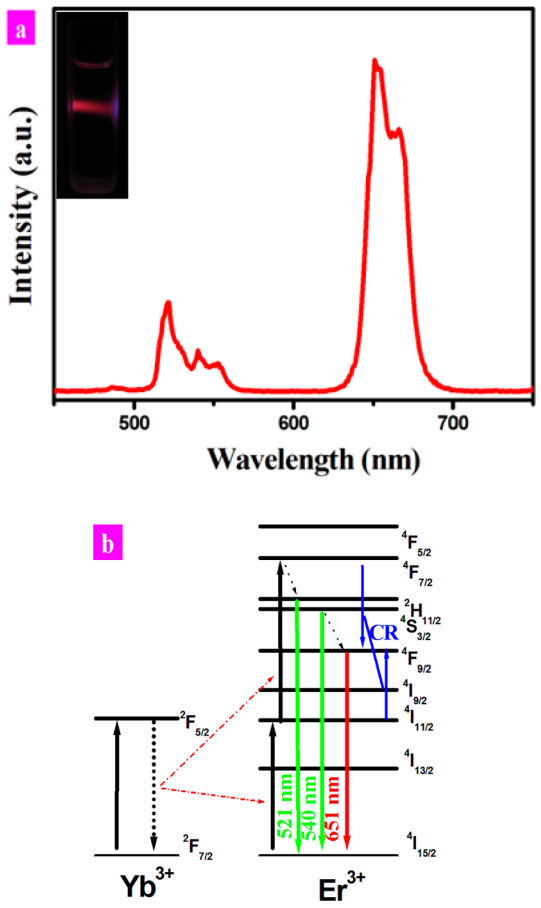

Figure 4. (a) UC spectrum of the amine-functionalized $NaYbF_4$:Er UCNPs and (b) schematic energy levels of Yb^{3+} and Er^{3+} ions (CR = cross-relaxation). The inset in panel a shows the digital photograph of the 1 wt % water solution of $NaYbF_4$:Er UCNPs under 980 nm excitation.

to adjacent Er^{3+}, resulting in $^4I_{15/2} \rightarrow {}^4I_{11/2}$ and $^4I_{11/2} \rightarrow {}^4F_{7/2}$ transitions of Er^{3+}. Subsequently, the excited electrons in the Er^{3+}:$^4F_{7/2}$ level non-radiatively relax to the $^4H_{11/2}$, $^4S_{3/2}$, and $^4F_{9/2}$ levels and generate the corresponding green and red emissions by radiative relaxation at 521, 540, and 651 nm, respectively. The inset of Figure 4a shows the digital photograph of the 1 wt % water solution of the amine-functionalized $NaYbF_4$:Er UCNPs under the excitation of the 980 nm laser with a power density of 5 W/cm^2. The intense eye-visible red luminescence can be observed. The dominant red UC emissions in $NaYbF_4$:Er UCNPs are mainly attributed to the cross-relaxation (CR) process ($^4F_{7/2} \rightarrow {}^4F_{9/2}$ and $^4F_{9/2} \leftarrow {}^4I_{11/2}$) of Er^{3+}. The higher Yb^{3+} concentration makes a more efficient CR process[58] occur and subsequently enhances the electron numbers in the Er^{3+}:$^4F_{9/2}$ level, resulting in the enhancement of red UC emission at 651 nm. The dominant red emission is more beneficial to achieve high-contrast imaging and deeper penetration depth for optical bioimaging in the biomedical area.

3.4. *In Vitro* UC Luminescence Bioimaging of HeLa Cells. To reveal the feasibility of the amine-functionalized $NaYbF_4$:Er UCNPs for optical bioimaging, the cell uptake and internalization of these UCNPs in HeLa cells were evaluated. HeLa cells were treated with the amine-functionalized $NaYbF_4$:Er UCNPs (200 μg/mL) at 37 °C and 5% CO_2 for 24 h and imaged by confocal fluorescent microscopy upon 980 nm excitation. Two typical imaging channels, including green (500−600 nm) and red (600−700 nm), were selected for optical bioimaging. Figure 5 shows the bright-field and UC luminescence images of the HeLa cells treated with UCNPs. As shown in panels a and d of Figure 5, HeLa cells can be readily distinguished by the bright-field image. Under 980 nm excitation, HeLa cells present a significant green UC signal (panels b and e of Figure 5) and intense red UC signal (panels c and f of Figure 5), indicating the successful cell uptake of these UCNPs in HeLa cells. The insets in panels b and c of Figure 5 are the corresponding localized emission spectra taken from HeLa cells and background. As demonstrated in the localized emission spectra, the characteristic green and intense red UC luminescence peaks at 540 and 651 nm were observed, which is in agreement with the aforementioned UC spectrum (Figure 4a), further confirming that the amine-functionalized UCNPs successfully internalized into HeLa cells. More importantly, a complete absence of autofluorescence was detected in the imaging spectral range from 500 to 700 nm. These results suggest that the amine-functionalized $NaYbF_4$:Er UCNPs are ideal probes for high-contrast *in vitro* UC luminescence imaging of cells with the absence of any autofluorescence.

3.5. Cell Toxicity Test. Low cell toxicity of these UCNPs is required for successful biomedical application. Therefore, to evaluate the cytotoxicity and biocompatible of these UCNPs, cell viability of these UCNPs in HeLa cells was measured using the standard MTT method (Figure 6). As demonstrated, cell viability was about 94% when treated with 200 μg/mL UCNPs. When the concentration of $NaYbF_4$:Er UCNPs was increased up to 500 μg/mL, cellular viability is 96%. With further increasing the concentration of UCNPs to 1000 μg/mL, the cellular viability is estimated to be 91%, indicating the remarkable low cytotoxicity of these UCNPs. Therefore, these UCNPs can be potentially used for high-contrast *in vitro* cell imaging with very low cytotoxicity.

3.6. *In Vivo* UC Bioimaging of a Mouse. To examine the feasibility of the amine-functionalized $NaYbF_4$:Er UCNPs for *in vivo* imaging, a nude mouse was subcutaneously injected with the amine-functionalized $NaYbF_4$:Er UCNPs (2 mg/mL, 200 μL). After injection, the mouse was imaged for *in vivo* UC bioimaging by the Bruker In-Vivo FX PRO *in vivo* imaging system under excitation of a fiber-coupled 980 nm laser. Figure 7 presents the *in vivo* whole-body images of a nude mouse with and without subcutaneous injection of the amine-functionalized $NaYbF_4$:Er UCNPs. Under excitation of the 980 nm laser, the *in vivo* imaging of the mouse without administration of UCNPs (Figure 7a) presents no optical signal, while high-contrast imaging of the mouse injected with UCNPs (Figure 7b) was observed, indicating that the as-prepared UCNPs can be applied to *in vivo* whole-body bioimaging.

3.7. Synergistic *in Vivo* X-ray and UC Bioimaging. Apart from the excellent UC, *in vitro*, and *in vivo* optical bioimaging properties, the amine-functionalized $NaYbF_4$:Er UCNPs can also be used as X-ray imaging contrast agents, owing to the large K-edge values and X-ray absorption coefficient of Yb^{3+}. As recent reported, Cui and co-workers have successfully developed Ln-doped $NaGdF_4$ for *in vivo* dual-modality imaging.[42] However, a synergistic combination of X-ray and UC bioimaging in a single system, as a new trend of bioimaging, can not only combine the advantages of both but also avoid the disadvantages of them. However, the synergistic *in vivo* X-ray and UC bioimaging based on $NaYbF_4$ UCNPs still

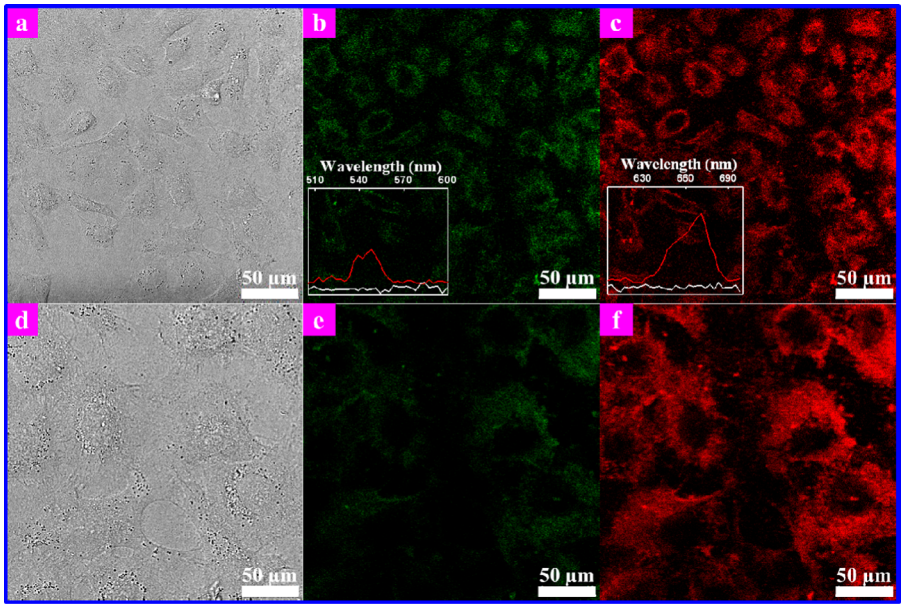

Figure 5. *In vitro* UC luminescence bioimaging of HeLa cells incubated with the $NaYbF_4$:Er UCNPs under excitation of a 980 nm laser: (a) bright-field image of HeLa cells, (b) green UC luminescence image (500−600 nm), (c) red UC fluorescent image (600−700 nm), (d, e, and f) high-magnification bright-field, green, and red UC images, respectively. The insets in panels b and c show the corresponding localized photoluminescence spectra taken from HeLa cells (red line) and background (white line), indicating the absence of any autofluorescence under the detected spectral regions from 500 to 700 nm.

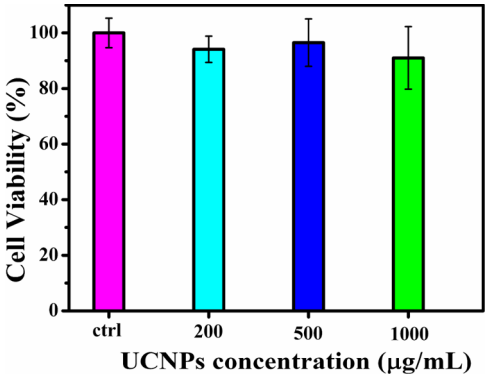

Figure 6. MTT assay for cell toxicity of the amine-functionalized $NaYbF_4$:Er UC nanoparticles in HeLa cells treated with different concentrations of these nanoparticles at 37 °C for 24 h under 5% CO_2. Error bars were based on triplicate samples.

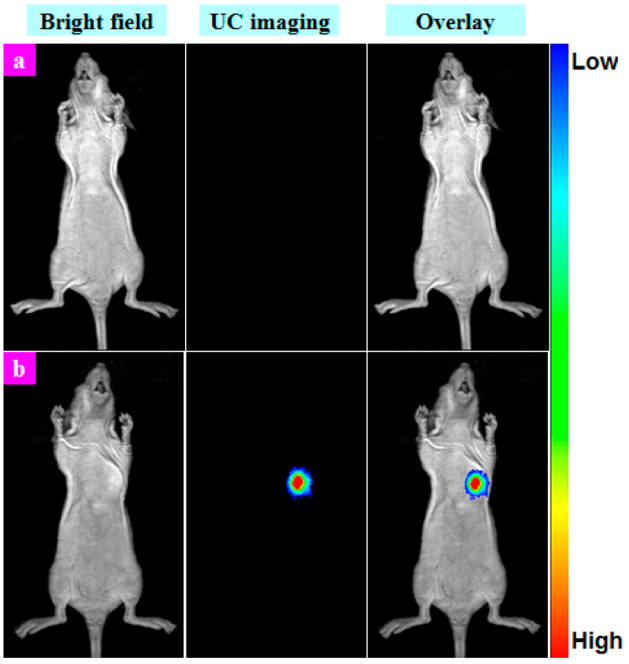

Figure 7. *In vivo* UC luminescence bioimaging of a nude mouse under the excitation of a 980 nm fiber-coupled laser: (a) without subcutaneous injection of the nanoparticles and (b) with subcutaneous injection of the nanoparticles. The left panel indicates the bright-field image; the middle panel denotes the UC luminescence image; and the right panel denotes the overlay image.

remained unexploited. To demonstrate the synergistic bioimaging of these UCNPs, a nude mouse was subcutaneously injected with physiological saline solution containing these UCNPs. After injection, a synergistic X-ray and UC bioimaging was performed using a multi-modal *in vivo* imaging system equipped with an external 980 nm fiber-coupled laser and X-ray imaging accessory. Figure 8 shows the synergistic dual-modality X-ray and UC imaging in a nude mouse. As demonstrated in Figure 8a, there are no X-ray and UC luminescence signals observed in the nude mouse without injecting UCNPs. After injection of UCNPs, the significant X-ray absorption contrast indicated by the red-dotted circle (the left panel of Figure 8b) was observed. Moreover, the UC luminescence signal with high contrast was also observed at the same region (the middle panel of Figure 8b). The overlay image (the right panel of Figure 8b) shows that the X-ray and UC signals were matched very well in the same region, indicating that the as-prepared UCNPs can be successfully used as synergistic dual-modality X-ray and UC luminescence bioimaging.

3.8. Tracking of These UCNPs in Nude Mice. It is significantly important to track the translocation of these UCNPs *in vivo*, which may provide valuable information for disease diagnosing and therapy. To reveal the biodistribution

dx.doi.org/10.1021/am500383m | *ACS Appl. Mater. Interfaces* 2014, 6, 3839−3846

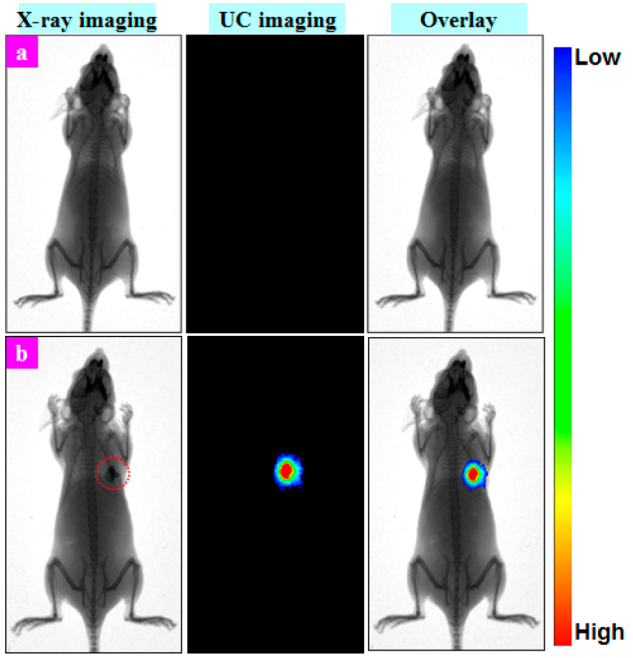

Figure 8. Synergistic *in vivo* X-ray and UC bioimaging of a nude mouse: (a) without injection of the nanoparticles and (b) with subcutaneous administration of the nanoparticles. The left panel indicates X-ray imaging; the middle panel denotes UC imaging; and the right panel denotes the overlay images. The X-ray signal is matched very well with the UC signal, indicating the synergistically combined two imaging modalities in one system.

and translocation of these UCNPs, *ex vivo* UC imaging of major organs (heart, lung, liver, spleen, and kidney) at different intravenous injection times was performed. As shown in Figure 9a, predominant and very weak UC signals were observed in

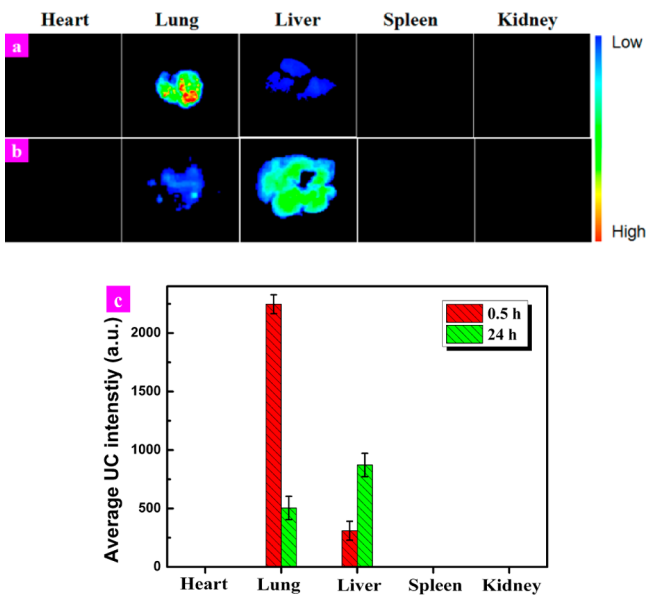

Figure 9. *Ex vivo* UC bioimaging of major organs from two mice intravenously injected with the nanoparticles after different times: (a) 0.5 h and (b) 24 h and (c) average UC luminescence intensity of organs. The significant translocation of nanoparticles from the lung into the liver after 24 h of injection was observed. Error bars were based on three mice per group.

the lung and liver, respectively, indicating that these UCNPs mainly accumulated in the lung after 0.5 h of systemic delivery. The firstly observed lung retention can be attributed to the amine-functional UCNPs interacting with the negative charges of capillary endothelial cells, which are displayed by plasmatic membranes[59] and the small size of the nanoparticle.[60] After 24 h of injection (Figure 9b), the UC signals of the lung were decreased and strong UC signals were observed in the liver, demonstrating the obvious translocation of these UCNPs from the lung to the liver. The average UC luminescence intensity shown in Figure 9c further evidenced the translocation of these UCNPs from the lung into the liver. Our findings, for the first time, suggest that the amine-functionalized $NaYbF_4$ UCNPs after systemic delivery would gradually migrate from the lung, where they initially accumulate, into the liver, which is consistent with the previous study.[60]

4. CONCLUSION

In conclusion, the amine-functionalized $NaYbF_4$:Er UCNPs with monodispersity and size of 28 nm were synthesized by a simple one-step hydrothermal method. The as-prepared $NaYbF_4$:Er UCNPs present dominant red and weaker green UC emissions, which is beneficial for optical bioimaging. The *in vitro* bioimaging and localized emission spectra taken from HeLa cells and background show that the amine-functionalized $NaYbF_4$:Er UCNPs can be successfully used as probes for UC luminescence bioimaging with high contrast and the absence of autofluorescence. In addition, the cytotoxicity of these UCNPs is remarkably low, even at a high concentration of 1000 μg/mL of UCNPs. Furthermore, these UCNPs were successfully applied in *in vivo* UC luminescence bioimaging of a mouse. As an added benefit, the amine-functionalized $NaYbF_4$:Er UCNPs can also be used as a new X-ray imaging agent, owing to the large X-ray absorption coefficient of the Yb element. After subcutaneous injection, a synergistic X-ray and UC luminescence bioimaging was firstly realized using a single compound of UCNPs. Obvious translocation of these UCNPs from the lung into the liver was observed. Therefore, the realized synergistic X-ray and UC luminescence imaging of our developed amine-functionalized $NaYbF_4$:Er UCNPs will provide promise for their wide applications in biomedical imaging by the combination of multi-modality imaging functionality.

AUTHOR INFORMATION

Corresponding Authors

*E-mail: songjunz@hunnu.edu.cn.
*E-mail: jh.hao@polyu.edu.hk.

Notes

The authors declare no competing financial interest.

ACKNOWLEDGMENTS

This work was supported by the National Natural Science Foundation of China (51102202 and 91230116), the Specialized Research Fund for the Doctoral Program of Higher Education of China (20114301120006), the Hunan Provincial Natural Science Foundation of China (12JJ4056), and the Scientific Research Fund of Hunan Provincial Education Department (13B062), China.

REFERENCES

(1) Hilderbrand, S. A.; Weissleder, R. Near-infrared fluorescence: Application to *in vivo* molecular imaging. *Curr. Opin. Chem. Biol.* **2010**, *14*, 71−79.

(2) Zhou, J.; Liu, Z.; Li, F. Y. Upconversion nanophosphors for small-animal imaging. *Chem. Soc. Rev.* **2012**, *41*, 1323−1349.

(3) Liu, Q.; Feng, W.; Yang, T. S.; Yi, T.; Li, F. Y. Upconversion luminescence imaging of cells and small animals. *Nat. Protoc.* **2013**, *8*, 2033−2044.

(4) Pan, L. Y.; He, M.; Ma, J. B.; Tang, W.; Gao, G.; He, R.; Su, H. C.; Cui, D. X. Phase and size controllable synthesis of $NaYbF_4$ nanocrystals in oleic acid/ionic liquid two-phase system for targeted fluorescent imaging of gastric cancer. *Theranostics* **2013**, *3*, 210−222.

(5) Wang, K.; Ma, J. B.; He, M.; Gao, G.; Xu, H.; Sang, J.; Wang, Y. X.; Zhao, B. Q.; Cui, D. X. Toxicity assessments of near-infrared upconversion luminescent LaF_3:Yb,Er in early development of zebrafish embryos. *Theranostics* **2013**, *3*, 258−266.

(6) Fan, W. P.; Shen, B.; Bu, W. B.; Chen, F.; Zhao, K. L.; Zhang, S. J.; Zhou, L. P.; Peng, W. J.; Xiao, Q. F.; Xing, H. Y.; Liu, J. N.; Ni, D. L.; He, Q. J.; Shi, J. L. Rattle-structured multifunctional nanotheranostics for synergetic chemo-/radiotherapy and simultaneous magnetic/luminescent dual-mode imaging. *J. Am. Chem. Soc.* **2013**, *135*, 6494−6503.

(7) Xiao, Q. F.; Zheng, X. P.; Bu, W. B.; Ge, W. Q.; Zhang, S. J.; Chen, F.; Xing, H. Y.; Ren, Q. G.; Fan, W. P.; Zhao, K. L.; Hua, Y. Q.; Shi, J. L. A core/satellite multifunctional nanotheranostic for *in vivo* imaging and tumor eradication by radiation/photothermal synergistic therapy. *J. Am. Chem. Soc.* **2013**, *135*, 13041−13048.

(8) Haase, M.; Schäfer, H. Upconverting nanoparticles. *Angew. Chem., Int. Ed.* **2011**, *50*, 5808−5829.

(9) Li, C. X.; Lin, J. Rare earth fluoride nano-/microcrystals: Synthesis, surface modification and application. *J. Mater. Chem.* **2010**, *20*, 6831−6847.

(10) Xia, A.; Chen, M.; Gao, Y.; Wu, D. M.; Feng, W.; Li, F. Y. Gd^{3+} complex-modified $NaLuF_4$-based upconversion nanophosphors for trimodality imaging of NIR-to-NIR upconversion luminescence, X-ray computed tomography and magnetic resonance. *Biomaterials* **2012**, *33*, 5394−5405.

(11) Wang, F.; Han, Y.; Lim, C. S.; Lu, Y. H.; Wang, J.; Xu, J.; Chen, H. Y.; Zhang, C.; Hong, M. H.; Liu, X. G. Simultaneous phase and size control of upconversion nanocrystals through lanthanide doping. *Nature* **2010**, *463*, 1061−1065.

(12) Wang, F.; Deng, R. R.; Wang, J.; Wang, Q. X.; Han, Y.; Zhu, H. M.; Chen, X. Y.; Liu, X. G. Tuning upconversion through energy migration in core−shell nanoparticles. *Nat. Mater.* **2011**, *10*, 968−973.

(13) Vetrone, F.; Naccache, R.; Mahalingam, V.; Morgan, C. G.; Capobianco, J. A. The active-core/active-shell approach: A strategy to enhance the upconversion luminescence in lanthanide-doped nanoparticles. *Adv. Funct. Mater.* **2009**, *19*, 2924−2929.

(14) Zhu, X. J.; Zhou, J.; Chen, M.; Shi, M.; Feng, W.; Li, F. Y. Core−shell Fe_3O_4@$NaLuF_4$:Yb,Er/Tm nanostructure for MRI, CT and upconversion luminescence tri-modality imaging. *Biomaterials* **2012**, *33*, 4618−4627.

(15) Buston, J. E. H.; Young, J. R.; Anderson, H. L. Rotaxane-encapsulated cyanine dyes: Enhanced fluorescence efficiency and photostability. *Chem. Commun.* **2000**, *11*, 905−906.

(16) Heim, R.; Cubitt, A. B.; Tsien, R. Y. Improved green fluorescence. *Nature* **1995**, *373*, 663−664.

(17) Gao, J. H.; Chen, K.; Xie, R. G.; Xie, J.; Lee, S.; Cheng, Z.; Peng, X. G.; Chen, X. Y. Ultrasmall near-infrared non-cadmium quantum dots for *in vivo* tumor imaging. *Small* **2010**, *6*, 256−261.

(18) Liu, Q.; Sun, Y.; Yang, T. S.; Feng, W.; Li, C. G.; Li, F. Y. Sub-10 nm hexagonal lanthanide-doped $NaLuF_4$ upconversion nanocrystals for sensitive bioimaging *in vivo*. *J. Am. Chem. Soc.* **2011**, *133*, 17122−17125.

(19) Zeng, S. J.; Tsang, M. K.; Chan, C. F.; Wong, K. L.; Fei, B.; Hao, J. H. Dual-modal fluorescent/magnetic bioprobes based on small sized upconversion nanoparticles of amine-functionalized $BaGdF_5$:Yb/Er. *Nanoscale* **2012**, *4*, 5118−5124.

(20) Wang, Y. F.; Liu, G. Y.; Sun, L. D.; Xiao, J. W.; Zhou, J. C.; Yan, C. H. Nd^{3+}-Sensitized upconversion nanophosphors: Efficient *in vivo* bioimaging probes with minimized heating effect. *ACS Nano* **2013**, *7*, 7200−7206.

(21) Zeng, S. J.; Tsang, M. K.; Chan, C. F.; Wong, K. L.; Hao, J. H. PEG modified $BaGdF_5$:Yb/Er nanoprobes for multi-modal upconversion fluorescent, *in vivo* X-ray computed tomography and biomagnetic imaging. *Biomaterials* **2012**, *33*, 9232−9238.

(22) Zhou, J. C.; Yang, Z. L.; Dong, W.; Tang, R. J.; Sun, L. D.; Yan, C. H. Bioimaging and toxicity assessments of near-infrared upconversion luminescent $NaYF_4$:Yb,Tm nanocrystals. *Biomaterials* **2011**, *32*, 9059−9067.

(23) Chatteriee, D. K.; Rufalhah, A. J.; Zhang, Y. Upconversion fluorescence imaging of cells and small animals using lanthanide doped nanocrystals. *Biomaterials* **2008**, *29*, 937−943.

(24) Xie, X. J.; Gao, N. Y.; Deng, R. R.; Sun, Q.; Xu, Q. H.; Liu, X. G. Mechanistic investigation of photon upconversion in Nd^{3+}-sensitized core-shell nanoparticles. *J. Am. Chem. Soc.* **2013**, *135*, 12608−12611.

(25) He, L.; Feng, L. Z.; Cheng, L.; Liu, Y. M.; Li, Z. W.; Peng, R.; Li, Y. G.; Guo, L.; Liu, Z. Multilayer dual-polymer-coated upconversion nanoparticles for multimodal imaging and serum-enhanced gene delivery. *ACS Appl. Mater. Interfaces* **2013**, *5*, 10381−10388.

(26) Wang, Z. L.; Hao, J. H.; Chan, H. L. W.; Wong, W. T.; Wong, K. L. A strategy for simultaneously realizing the cubic-to-hexagonal phase transition and controlling the small size of $NaYF4:Yb^{3+},Er^{3+}$ nanocrystals for in vitro cell imaging. *Small* **2012**, *8*, 1863−1868.

(27) Liu, H. R.; Lu, W.; Wang, H. B.; Rao, L.; Yi, Z. G.; Zeng, S. J.; Hao, J. H. Simultaneous synthesis and amine-functionalization of single-phase $BaYF_5$:Yb/Er nanoprobe for dual-modal *in vivo* upconversion fluorescence and long-lasting X-ray computed tomography imaging. *Nanoscale* **2013**, *5*, 6023−6029.

(28) Cheng, L.; Yang, K.; Zhang, S. A.; Shao, M. W.; Lee, S. T.; Liu, Z. Highly-sensitive multiplexed *in vivo* imaging using PEGylated upconversion nanoparticles. *Nano Res.* **2010**, *3*, 722−732.

(29) Mader, H. S.; Kele, P.; Saleh, S. M.; Wolfbeis, O. S. Upconverting luminescent nanoparticles for use in bioconjugation and bioimaging. *Curr. Opin. Chem. Biol.* **2010**, *14*, 582−596.

(30) Shen, J.; Chen, G. Y.; Vu, A. M.; Fan, W.; Bilsel, O. S.; Chang, C. C.; Han, G. Engineering the upconversion nanoparticle excitation wavelength: Cascade sensitization of tri-doped upconversion colloidal nanoparticles at 800 nm. *Adv. Opt. Mater.* **2013**, *1*, 644−650.

(31) Dai, Y. L.; Ma, P. A.; Cheng, Z. Y.; Kang, X. J.; Zhang, X.; Hou, Z. Y.; Li, C. X.; Yang, D. M.; Zhai, X. F.; Lin, J. Up-conversion cell imaging and pH-induced thermally controlled drug release from $NaYF_4$:Yb^{3+}/Er^{3+}@hydrogel core−shell hybrid microspheres. *ACS Nano* **2012**, *6*, 3327−3338.

(32) Cheng, L.; Yang, K.; Li, Y. G.; Chen, J. H.; Wang, C.; Shao, M. W.; Lee, S. T.; Liu, Z. Facile preparation of multifunctional upconversion nanoprobes for multimodal imaging and dual-targeted photothermal therapy. *Angew. Chem., Int. Ed.* **2011**, *50*, 7385−7390.

(33) Gao, G.; Zhang, C. L.; Zhou, Z. J.; Zhang, X.; Ma, J. B.; Li, C.; Jin, W. L.; Cui, D. X. One-pot hydrothermal synthesis of lanthanide ions doped one-dimensional upconversion submicrocrystals and their potential application *in vivo* CT imaging. *Nanoscale* **2013**, *5*, 351−362.

(34) Gao, D. L.; Zhang, X. Y.; Gao, W. Formation of bundle-shaped β-$NaYF_4$ upconversion microtubes via ostwald ripening. *ACS Appl. Mater. Interfaces* **2013**, *5*, 9732−9739.

(35) Zhou, J.; Yu, M. X.; Sun, Y.; Zhang, X. Z.; Zhu, X. J.; Wu, Z. H.; Wu, D. M.; Li, F. Y. Fluorine-18-labeled Gd^{3+}/Yb^{3+}/Er^{3+} co-doped $NaYF_4$ nanophosphors for multimodality PET/MR/UCL imaging. *Biomaterials* **2011**, *32*, 1148−1156.

(36) Vetrone, F.; Naccache, R.; Juarranz de la Fuente, A.; Sanz-Rodríguez, F.; Blazquez-Castro, A.; Rodriguez, E. M.; Jaque, D.; Sole, J. G.; Capobianco, J. A. Intracellular imaging of HeLa cells by non-functionalized $NaYF_4$:Er^{3+},Yb^{3+} upconverting nanoparticles. *Nanoscale* **2010**, *2*, 495−498.

(37) Zhou, J.; Sun, Y.; Du, X. X.; Xiong, L. Q.; Hu, H.; Li, F. Y. Dual-modality *in vivo* imaging using rare-earth nanocrystals with near-

infrared to near-infrared (NIR-to-NIR) upconversion luminescence and magnetic resonance properties. *Biomaterials* **2010**, *31*, 3287−3295.
(38) Qiu, P. Y.; Zhou, N.; Chen, H. Y.; Zhang, C. L.; Gao, G.; Cui, D. X. Recent advances in lanthanide-doped upconversion nanomaterials: Synthesis, nanostructures and surface modification. *Nanoscale* **2013**, *5*, 11512−11525.
(39) He, M.; Huang, P.; Zhang, C. L.; Ma, J. B.; He, R.; Cui, D. X. Phase- and size-controllable synthesis of hexagonal upconversion rare-earth fluoride nanocrystals through an oleic acid/ionic liquid two-phase system. *Chem.—Eur. J.* **2012**, *18*, 5954−5969.
(40) Nyk, M.; Kumar, R.; Ohulchanskyy, T. Y.; Bergey, E. J.; Prasad, P. N. High contrast *in vitro* and *in vivo* photoluminescence bioimaging using near infrared to near infrared up-conversion in Tm^{3+} and Yb^{3+} doped fluoride nanophosphors. *Nano Lett.* **2008**, *8*, 3834−3838.
(41) Ma, J. B.; Huang, P.; He, M.; Pan, L. Y.; Zhou, Z. J.; Feng, L. L.; Gao, G.; Cui, D. X. Folic acid-conjugated LaF_3:Yb,Tm@SiO_2 nanoprobes for targeting dual-modality imaging of upconversion luminescence and X-ray computed tomography. *J. Phys. Chem. B* **2012**, *116*, 14062−14070.
(42) He, M.; Huang, P.; Zhang, C. L.; Hu, H. Y.; Bao, C. C.; Gao, G.; He, R.; Cui, D. X. Dual phase-controlled synthesis of uniform lanthanide-doped $NaGdF_4$ upconversion nanocrystals via an OA/ionic liquid two-phase system for *in vivo* dual-modality imaging. *Adv. Funct. Mater.* **2011**, *21*, 4470−4477.
(43) Kramer, K. W.; Biner, D.; Frei, G.; Gudel, H. U.; Hehlen, M. P.; Luthi, S. R. Hexagonal sodium yttrium fluoride based green and blue emitting upconversion phosphors. *Chem. Mater.* **2004**, *16*, 1244−1251.
(44) Kumar, R.; Nyk, M.; Ohulchanskyy, T. Y.; Flask, C. A.; Prasad, P. N. Combined optical and MR bioimaging using rare earth ion doped $NaYF_4$ nanocrystals. *Adv. Funct. Mater.* **2009**, *19*, 853−859.
(45) Li, Z. Q.; Zhang, Y.; Jiang, S. Multicolor core/shell-structured upconversion fluorescent nanoparticles. *Adv. Mater.* **2008**, *20*, 4765−4769.
(46) Wang, Z. L.; Hao, J. H.; Chan, H. L. W.; Law, G. L.; Wong, W. T.; Wong, K. L.; Murphy, M. B.; Su, T.; Zhang, Z. H.; Zeng, S. Q. Simultaneous synthesis and functionalization of water-soluble upconversion nanoparticles for *in-vitro* cell and nude mouse imaging. *Nanoscale* **2011**, *3*, 2175−2181.
(47) Li, Z. Q.; Zhang, Y. Monodisperse silica-coated polyvinylpyrrolidone/$NaYF_4$ nanocrystals with multicolor upconversion fluorescence emission. *Angew. Chem., Int. Ed.* **2006**, *45*, 7732−7735.
(48) Chen, G. Y.; Ohulchanskyy, T. Y.; Kumar, R.; Ågren, H.; Prasad, P. N. Ultrasmall monodisperse $NaYF_4$:Yb^{3+}/Tm^{3+} nanocrystals with enhanced near-infrared to near-infrared upconversion photoluminescence. *ACS Nano* **2010**, *4*, 3163−3168.
(49) Zeng, S. J.; Ren, G. Z.; Yang, Q. B. Fabrication, formation mechanism and optical properties of novel single-crystal Er^{3+} doped $NaYbF_4$ micro-tubes. *J. Mater. Chem.* **2010**, *20*, 2152−2156.
(50) Zeng, S. J.; Ren, G. Z.; Xu, C. F.; Yang, Q. B. Modifying crystal phase, shape, size, optical and magnetic properties of monodispersed multifunctional $NaYbF_4$ nanocrystals through lanthanide doping. *CrystEngComm* **2011**, *13*, 4276−4281.
(51) Wang, J.; Wang, F.; Wang, C.; Liu, Z.; Liu, X. G. Single-band upconversion emission in lanthanide-doped $KMnF_3$ nanocrystals. *Angew. Chem., Int. Ed.* **2011**, *50*, 10369−10372.
(52) http://physics.nist.gov/PhysRefData/XrayMassCoef/.
(53) Yu, S. B.; Watson, A. D. Metal-based X-ray contrast media. *Chem. Rev.* **1999**, *99*, 2353−2378.
(54) Liu, Y. L.; Ai, K. L.; Liu, J. H.; Yuan, Q. H.; He, Y. Y.; Lu, L. H. A high-performance ytterbium-based nanoparticulate contrast agent for *in vivo* X-ray computed tomography imaging. *Angew. Chem., Int. Ed.* **2012**, *51*, 1437−1442.
(55) Wang, F.; Liu, X. G. Upconversion multicolor fine-tuning: Visible to near-infrared emission from lanthanide-doped $NaYF_4$ nanoparticles. *J. Am. Chem. Soc.* **2008**, *130*, 5642−5643.
(56) Jin, J. F.; Gu, Y. J.; Man, C. W. Y.; Cheng, J. P.; Xu, Z. H.; Zhang, Y.; Wang, H. S.; Lee, V. H. Y.; Cheng, S. H.; Wong, W. T. Polymer-coated $NaYF_4$:Yb^{3+},Er^{3+} upconversion nanoparticles for charge-dependent cellular imaging. *ACS Nano* **2011**, *5*, 7838−7847.
(57) Ju, Q.; Tu, D. T.; Liu, Y. S.; Li, R. F.; Zhu, H. M.; Chen, J. C.; Chen, Z.; Huang, M. D.; Chen, X. Y. Amine-functionalized lanthanide-doped $KGdF_4$ nanocrystals as potential optical/magnetic multimodal bioprobes. *J. Am. Chem. Soc.* **2012**, *134*, 1323−1330.
(58) Vetrone, F.; Boyer, J. C.; Capobianco, J. A.; Speghini, A.; Bettinelli, M. Significance of Yb^{3+} concentration on the upconversion mechanisms in codoped Y_2O_3:Er^{3+},Yb^{3+} nanocrystals. *J. Appl. Phys.* **2004**, *96*, 661−667.
(59) Le Masne de Chermont, Q.; Chanéac, C.; Seguin, J.; Pellé, F.; Maîtrejean, S.; Jolivet, J. P.; Gourier, D.; Bessodes, M.; Scherman, D. Nanoprobes with near-infrared persistent luminescence for *in vivo* imaging. *Proc. Natl. Acad. Sci. U. S. A.* **2007**, *104*, 9266−9271.
(60) Wang, C.; Cheng, L.; Xu, H.; Liu, Z. Towards whole-body imaging at the single cell level using ultra-sensitive stem cell labeling with oligo-arginine modified upconversion nanoparticles. *Biomaterials* **2012**, *33*, 4872−4881.